A Comprehensive Single-Particle Model for Solid-State Polymerization of Poly(L-lactic acid)

Vimal Katiyar, Mallikarjun Sharada Shaama, Hemant Nanavati

Department of Chemical Engineering, Indian Institute of Technology Bombay, Powai, Mumbai 400 076, India

Received 24 April 2010; accepted 28 December 2010
DOI 10.1002/app.34061
Published online 6 July 2011 in Wiley Online Library (wileyonlinelibrary.com).

ABSTRACT: We propose here, a comprehensive model for the solid-state polymerization (SSP) of a low to moderate molecular weight (MW) prepolymer of lactic acid, to produce high MW poly(L-lactic acid) (PLLA). The reactions are rationally assumed to occur only in the amorphous region, and effective concentrations of end groups, vary with crystalinity, X_c, during SSP. We estimate byproduct diffusivities, D, using free volume theory. The effects of various parameters on the SSP of PLLA prepolymer have been examined with respect to the optimum MW, X_c and D. We introduce self-consistently, scaling factors of ~ 0.27, in the experimental procedure, to determine via ^{19}F-NMR, concentrations of the end groups, after converting them to fluorinated ester groups. The relevant reaction rate constants are obtained by fitting to early time data from representative SSP experiments at 150°C, under high vacuum, on PLLA prepolymer powder (i.e., spherical geometry) of number average MW, $\overline{M_{n0}} \sim 10{,}200$ Da, which attains $\overline{M_n} \sim 150{,}000$ Da, via SSP. The subsequent successful comparison of the model predictions with experimental data throughout the entire SSP duration indicates that the model is comprehensive and accounts for all the relevant phenomena occurring during the SSP to synthesize high MW PLLA. © 2011 Wiley Periodicals, Inc. J Appl Polym Sci 122: 2966–2980, 2011

Key words: poly(L-lactic acid); solid-state polymerization; kinetics (polymerization); modeling; byproduct diffusivity; free volume theory

INTRODUCTION

Biodegradable polymers such as poly(L-lactic acid) (PLLA) have received much attention, due to their extensive biomedical applications, and as a means to address environmental problems caused by conventional plastics. PLLAs excellent mechanical properties also give it immense potential as a commodity polymer.[1,2] Various attempts have been made to develop PLLA with targeted properties, which usually require high molecular weight (MW).[3] Solid-state polymerization (SSP) is an important, nonhazardous method, to synthesize high MW PLLA. The advantages of SSP include low operating temperatures, which reduce side reactions and thermal degradation, while permitting inexpensive equipment and implementation of uncomplicated and environmentally sound procedures. The disadvantage of SSP is its slow reaction kinetics, compared with melt-state polymerization.

Various reports on SSP and their kinetics models are reported in the literature for polyesters (e.g., poly(ethylene terephthalate); (PET),[4–8] PET with nanofillers,[9,10] poly(butylene terephthalate),[11] polycarbonates,[12,13] polyamides,[14–19] etc). These commercially important polymers are prepared mainly by melt polycondensation. Although there has been a recent report on the modeling of PLLA synthesis by melt polycondensation of lactic acid,[20] there is no report till date, on the modeling of the SSP of PLLA. Moon et al.[21] report the successful step-growth SSP of PLLA prepolymer, which yields high weight average MW (maximum $M_w \sim 600{,}000$ Da), where the prepolymer is also formed by step-growth polymerization of lactic acid precursor. Xu et al.[22] have reported the positive effect of precrystallization on PLLA MW during SSP. In contrast, Shinno et al.[23] have reported that the chain-growth SSP does not increase the MW of prepolymer synthesized by chain growth polymerization of L-lactide. Therefore, an understanding of the SSP mechanism and a comprehensive kinetics model to predict the influence of various parameters on the SSP rate of PLLA are long-standing problems and seek attention.

The kinetics models developed till date for polycondensation SSP reactions are classified into two groups: the Flory theory-based models and the power law models.[24] According to the Flory theory, the kinetics models describe propagating reaction kinetics of second order, assuming equal reactivities of the functional end groups, for reversible SSP reactions. Power law models basically correlate the rheological properties with the MW buildup during SSP.[25]

Correspondence to: H. Nanavati (hnanavati@che.iitb.ac.in).

SSP is a step growth polycondensation process, in which the terminal end groups of the growing polymer chains, react with each other, to form much longer chain molecules, with simultaneous removal of byproducts such as water. In addition, other effects occur simultaneously: these include (1) significant decrease in diffusivities of reactive end groups of polymer chains and of reaction byproducts, due to decrease in chain mobility, caused by MW and crystallinity (X_c) increase; and (2) although end-groups are consumed during SSP, this decrease in their effective concentrations in the amorphous region is countered by the decrease in the amorphous volume fraction, because crystallization occurs during SSP.

These effects play important roles in the kinetics of SSP and thus affect the determination of the reaction rate constants. However, information obtained from experiments is limited in terms of the mechanism, side reactions, and concentrations of reactive end groups and byproducts. We have incorporated these effects (based on information from our own experimental data,[26] which are based on the procedure by Moon et al.[21]) in our SSP modeling framework, so as to make it realistic for objective correlation with experimental results.

In the fringed-micelle morphology considered for the SSP of PLLA grains of both, spherical and cylindrical geometries, the overall SSP reaction rate depends on chemical (intrinsic rate constant) as well as physical processes (diffusion). Our modeling framework considers the following steps involved during SSP: (1) diffusion of the reactive hydroxyl and carboxylic acid end groups toward each other in the amorphous region, (2) reversible chemical reactions between these reactive chain end groups, (3) depolymerization to cyclic such as lactide, a major byproduct, (4) ester-exchange reactions between the entangled chains, (5) diffusion (diffusivities, D_j) of the volatile byproducts (water and lactide) within the solid polymer, and (6) diffusion of volatile byproducts, out from the polymer bulk through the surface (in inert gas or under vacuum). The last step leads to mass loss and a shift in the equilibrium, which are also accounted for in our framework.

In this work, we first list the various reactions and phenomena, and their governing equations. Then, we determine the relevant system properties (such as X_c and D_j) and their variation during the reaction as well as the chemical parameters such as the initial concentrations and reaction rate constants.

Diffusion coefficients for byproducts such as lactide and water have been obtained by the free volume (FV) approach. This geometry-based approach assumes that the diffusivities can be expressed as functions of the size and shape of the diffusing molecules, the volume fraction of the amorphous phase, and the reaction temperature. The initial crystallinity and its evolution are determined via Differential scanning calorimetry (DSC) of PLLA samples as described in the "Characterization" section, before and during SSP. The crystallinity data have been fit to the Avrami equation, which has been incorporated into the model to account for realistic evolution during SSP of the polymer morphology and effective amorphous end-group concentrations.

We also report the determination of initial concentrations (for SSP) of the hydroxyl and carboxylic acid, achieved by first fluorinating the end-groups of the PLLA prepolymer, and then by quantifying the fluorinated end groups, via ^{19}F-NMR. The quantification is achieved self-consistently, via scaling constants to correlate end group concentrations with the MW of the PLLA prepolymer. Kinetics parameters such as the rate constants for esterification, hydrolysis, and depolymerization have been accordingly assigned and calculated with respect to initial data of representative SSP experiments.[26]

By comparing the resulting model predictions with the experimental data corresponding to the entire SSP duration, we validate the enhanced model accuracy and provide an improved understanding of the mechanism of SSP.

Next, we describe briefly the experimental materials and procedure. The data from these experiments have been used in developing and validating the model framework reported here. This is followed by the modeling and the comparison of the model predictions with experimental data.

MATERIALS AND EXPERIMENTAL DETAILS

Materials

Stannous octoate ($Sn(Oct)_2$), $SnCl_2{\cdot}2H_2O$, *p*-toluene sulphonic acid, 1,3-dicyclohexylcarbodiimide (DCC), hexafluoroisopropanol (HFIP), 4-pyrrolidinopyridine (PDP), trifluorotoluene (TFT), trifluoro acetic acid (TFA), and deuterated chloroform ($CDCl_3$) have been purchased from Sigma Aldrich. L-lactic acid (PH-90) has been purchased from Purac (The Netherlands). Chloroform, methanol, and toluene have been used, as supplied by Merck Chemicals, India.

Synthesis and SSP of PLLA prepolymer

This section describes the experimental procedures for (i) PLLA prepolymer synthesis by MP of lactic acid, via lactic acid oligomer (OLLA) intermediate, followed by SSP of Pre-PLLA, (ii) fluoroderivatization procedures for terminal hydroxyl and carboxylic acid for ^{19}F-NMR based determination of end-group concentration. The MWs determined at each PLLA synthesis step, have been obtained by Gel

permeation chromatography (GPC), as described in the "Characterization" section.

PLLA prepolymer synthesis by MP of lactic acid/ SSP of prepolymer

We use a three-necked tubular reactor, with a condenser and receiver at opposite ends and with a screw impeller based mechanical stirrer. We added $\sim$ 400 g of lactic acid (90% w/w solution in water) and solution is then stirred at 30 rpm under nitrogen flow, and subsequently, the temperature is maintained to 150°C for 2 h by a temperature-controlled tubular heater. We continue stirring at 150°C but gradually reduce pressure for the next 4 h. The molten reaction mixture is allowed to cool to room temperature, and we obtain $\sim$ 300 g (yield $\sim$ 82%) OLLA of number average MW, $\overline{M_n} \sim$ 1500 Da, and polydispersity index (PDI) $\sim$ 1.06. 30 gm of this OLLA is further stirred at 35 rpm and heated to 180°C by the temperature-controlled tubular heater for 15 min, under nitrogen flow. Subsequently, we add the binary catalyst which includes equimolar *p*-toluenesulfonic acid and tin chloride dehydrate. Prepolymer synthesized by polymerization under high vacuum for 4 h is of MW, $\overline{M_{n0}} =$ 10,200 Da.

SSP is performed on the the PLLA prepolymer powder. Two grams of the prepolymer is taken in a flame dried tubular glass reactor having diameter of 20 cm, connected with a vacuum line (10^{-3} torr) through a glass adapter valve. First, the prepolymer is subject to vacuum at 105°C for 2 h. SSP is then performed for predetermined times of 5–20 h at 150°C, by immersing the glass reactor in an oil bath.

Fluoroderivatization of terminal acid and hydroxyl groups in PLLA prepolymer to determine terminal group concentrations

The fluoroderivatization of the prepolymer terminal acid groups is carried out by DCC mediated esterification with HFIP. One chip of the prepolymer (0.045 g) is dissolved in a mixture of HFIP (0.2 g) and $CDCl_3$ (1.0 g) at room temperature. First, 0.1 g of a solution of 0.001-g PDP in 1.0-g $CDCl_3$ is added, followed by 0.2 g of a solution of 0.0075-g DCC in 1.5-g $CDCl_3$. Finally, 0.1 g of a solution of 0.01-g TFT in 2.0-g $CDCl_3$ is added to the above reaction mixture, to yield the sample for ^{19}F-NMR analysis.

The hydroxyl end-groups of the prepolymer are fluoroderivatized by esterification with TFA. One chip of PLLA prepolymer (0.045 g) is dissolved in a mixture of TFA (0.2 g) and $CDCl_3$ (1.0 g). A total of 0.1 g of solution of 0.01-g TFT in 2.0-g $CDCl_3$ is added to the above reaction mixture. Samples are kept for 48 h. Subsequently, the ^{19}F-NMR analysis is carried out.

Characterization

NMR analysis

^{19}F-NMR measurements (400 MHz) have been carried out on a Varian VXR-400, to determine the end groups conversion, for quantification of hydroxyl and carboxyl end groups.

Gel permeation chromatography (GPC)

The $\overline{M_w}$, $\overline{M_n}$, and PDI of PLLA are determined by a Waters GPC (Waters 2414 RI Detector) with PL-gel, 5 μ Mixed-D (2 × 300 mm^2) column, with polystyrene standards in chloroform, for MW up to 400,000 Da.

Differential scanning calorimetry (DSC)

The enthalpy of crystallization (ΔH_c), enthalpy of melting (ΔH_m), and crystallinity (X_c) of PLLA have been determined by a NETZSCH STA 409PC Luxx Differential Scanning Calorimeter, in the temperature range, 25–300°C, at 10°C/min. To compute X_c, we subtract from the total endothermic heat flow during the melting of all crystallites, the extra heat, if any, which would be attributed to melting of crystallites, formed during the heating scan. The melt enthalpy considered for 100% crystalline PLLA is 93 J/g.[1]

ASSUMPTIONS AND MODELING

This modeling approach accounts for the polymer chain length growth, to establish a framework and to represent the reaction kinetics. We use a functional group-based approach, to establish the overall network of reactions.[27,28] Polymerization reactions can be regarded as reactions between the hydroxyl and carboxylic acid end groups, of the growing PLLA chains. All the components considered in the reaction scheme are listed in Table I; the two terminal (—OH, —COOH) groups, the bonded ester group and water and lactide byproducts, are expressed as $(LA)_a$—OH, $(LA)_a$—COOH, $HO(LA)_aCOOH$, W, and $(LA)_2$, respectively.

The complete set of possible reactions considered is presented in Table II. In this table, k_1 and k_2 are the respective rate constants of the polycondensation and hydrolysis reactions (no. 1), k_3 is the depolymerization constant for the polymer backbiting side reaction, which yields lactide (no. 2), and k_4 and k_5 are the rate constants for transesterification (no. 3) and ester exchange reactions (no. 4), respectively.

During SSP, the unsteady–state diffusion of the volatile byproducts such as lactide and water is coupled with chemical reaction. We assume the diffusion process to be Fickian and isothermal, without change in particle volume. The mass balance equations of components *j*, including $(LA)_2$ and W in the spherical PLLA particle, can be written as follows.

TABLE I
Molecular Structure of Components Occurring in the Modeling Framework

Symbol	Descriptions	Molecular structure
$(LA)_a$—OH	PLLA: terminal-OH group	—COOCH(CH_3) OH
$(LA)_a$—COOH	PLLA: terminal-COOH group	—OCH(CH_3)COOH
$HO(LA)_aCOOH$	PLLA: bonded ester group	—COO—
W	Byproduct: water	H_2O
$(LA)_2$	Depolymerization product: lactide	$C_6H_8O_4$

$$\frac{\partial C_j}{\partial t} = D_j\left[\frac{\partial^2 C_j}{\partial r^2} + \frac{m}{r}\frac{\partial C_j}{\partial r}\right] + G_j(t) \quad (1)$$

where C_j and D_j are the concentrations and diffusivities, respectively, of the byproducts j (lactide and water), in the semicrystalline polymer, t is reaction time, and r is the radial distance from the origin of the sphere ($m = 2$) or from the cylinder axis ($m = 1$), i.e., in the direction of diffusion. $G_j(t)$ is the generation rate due to chemical reactions and can be written as a concentration-dependent reaction rate expression.

The mass balance equations of nondiffusing components can be written by removing the diffusion terms in eq. (1):

$$\frac{dC_j}{dt} = G_j(t) \quad (2)$$

In the rate expressions, we have incorporated the assumption that the entire SSP reaction takes place only in the amorphous region, because the end-groups are restricted to this region. Therefore, all the generation steps are calculated on the basis of the amorphous fraction (Φ_A) only, and the time-dependent crystallization effects are incorporated into the concentration terms; i.e., the concentrations of end groups and ester groups are modified, as shown in eqs. (3) and (4):

$$C_j' = \frac{C_j}{\Phi_A} \quad (3)$$

$$G_j'(t) = \frac{G_j(t)}{\Phi_A} \quad (4)$$

Generation rates of nondiffusing components such as $(LA)_a$—OH, $(LA)_a$—COOH, $HO(LA)_aCOOH$ as well as diffusing components W and $(LA)_2$, are listed in Table III.

The generation rates of both, nondiffusing and diffusing components, are not affected by reactions 3 and 4 of Table II. These equations describe mutual interchanges in the sequences of the growing PLLA chains, which do not contribute toward the number average molecular weight ($\overline{M_n}$).

The relevant boundary conditions for both, spherical and cylindrical geometries (particle radius = r_s), are:

$$\frac{\partial C_j}{\partial r} = 0 \quad \text{for } t > 0,\ r = 0 \quad (5)$$

$$C_j = C_j^S \quad \text{for } t > 0,\ r = r_S \quad (6)$$

$$C_j = C_j^0 \quad \text{for } t = 0,\ 0 < r < r_S \quad (7)$$

In eqs. (1)–(7), species j are $(LA)_a$—OH, $(LA)_a$—COOH, $HO(LA)_aCOOH$, W, and $(LA)_2$. In addition, eq. (6) is required only for W and $(LA)_2$. Initial concentrations, C_j^0, of nondiffusing terminal groups [eq. (7)] have been estimated by ^{19}F-NMR and also from prepolymer MW data. However, initial concentrations of W and $(LA)_2$ are assumed to be zero, because of the high vacuum imposed on the prepolymer, before SSP. C_j are the concentrations based on the entire volume of the pellet, and C_j^i are the corresponding effective concentrations in the amorphous region. In case of [COO], only the amorphous phase units participate in the reactions. Therefore, eqs. (3) and (4) are not applicable for [COO]; i.e., $C'_{COO} = C_{COO}$.[27]

In this framework, we have assumed a quasi-steady state for Φ_A. Hence, although the numerical method has incorporated the instantaneous value of Φ_A during the SSP, the differentials in Table III consider Φ_A as a constant. A refinement of our framework could consider a more rigorous incorporation of Φ_A in the differentials of Table III.

TABLE II
Reactions Considered for Modeling SSP

No.	Reactions	Rate constants
1	$(LA)_a$—OH + $(LA)_b$—COOH $\rightleftarrows$ HOOC—$(LA)_{a+b}$—OH + W	k_1, k_2
2	$(LA)_a$—OH → $(LA)_{a-2}$—OH + (LA)	k_3
3	$(LA)_a$—OH + HOOC—$(LA)_c$—OH → HOOC—$(LA)_{a+x}$—OH + $(LA)_{c-x}$—COOH	k_4
4	HOOC—$(LA)_d$—OH + HOOC—$(LA)_e$—OH → HOOC—$(LA)_{d'}$—OH + HOOC—$(LA)_{e'}$—OH	k_5

TABLE III
Generation Rates Used in the Model for Diffusing and Nondiffusing Components

1	$\frac{dC_{COOH}}{dt} = -2k_1\frac{C_{COOH}^2}{\Phi_A} + k_2 C_{COO} C_W$
2	$\frac{dC_{OH}}{dt} = -2k_1\frac{C_{OH}^2}{\Phi_A} + k_2 C_{COO} C_W$
3	$\Phi_A\frac{dC_{COO}}{dt} = 2k_1\frac{C_{OH}^2}{\Phi_A} - k_2 C_{COO} C_W - 2k_3 C_{OH}$
4	$\frac{\partial C_{(LA)_2}}{\partial t} = D_{(LA)_2}\left[\frac{\partial^2 C_{(LA)_2}}{\partial r^2} + \frac{m}{r}\frac{\partial C_{(LA)_2}}{\partial r}\right] + 2k_1\frac{C_{OH}^2}{\Phi_A} - k_2 C_{COO} C_{(LA)_2}$
5	$\frac{\partial C_W}{\partial t} = D_W\left[\frac{\partial^2 C_W}{\partial r^2} + \frac{m}{r}\frac{\partial C_W}{\partial r}\right] + 2k_1\frac{C_{OH}^2}{\Phi_A} - k_2 C_{COO} C_W$

In the sections that follow, we first describe the modeling of the physical effects, i.e., byproduct diffusion and crystallization (as well as initial crystallinity). This is followed by determination of the terminal group concentration by ^{19}F-NMR. We then determine the rate constants by fitting to initial time data of the SSP reaction. These data form the inputs to the final kinetics modeling, and MW build-up. We then discuss all the results and their implications, and compare with experimental data, the predictions of our comprehensive modeling.

DETERMINATION OF DIFFUSION COEFFICIENTS

We now determine the diffusion coefficients, D_j, of the byproducts and some of the carrier gases, j, by the FV approach.[29] The FV theory of diffusion, postulates that the diffusivity of a molecule in a medium, is related to the redistribution of the FV, and hence, to the molecular mobility in the medium. This method has been successfully implemented previously[27–29] for the polymer-diffusant system, during the SSP of PET. According to this theory, the diffusion coefficient of a gaseous molecule in a concentrated polymer solution, is given by:

$$D_j = RTA_j \exp\left[-\frac{B_j}{V_j}\right] \quad (8)$$

where D_j is the diffusion coefficient of molecule type j, R is the gas constant, T is temperature (K); A_j (prefactor) and B_j (jump factor) are constants, whose values depend on the size and shape of the diffusing molecules. In particular, B_j is a measure of the minimum size required of the hole, to accommodate the diffusing molecules. Therefore, it is anticipated that $\ln(B_j)$ is a linear function of the square of the molecular diameter or the hydrodynamic radius, of the diffusant. Equation (8) postulates that the diffusion coefficient is an exponential function of effective fractional FV, V_f.

$$V_f = f_A\Phi_A + f_{(LA)_2}\Phi_{(LA)_2} + f_W\Phi_W \quad (9)$$

where the amorphous volume fraction, Φ_A, varies with SSP time. f_A, $f_{(LA)_2}$, and f_W denote the fractional FVs of the amorphous phase, lactide and water, respectively. As the volume fractions of lactide, $\Phi_{(LA)_2}$, and of water, Φ_W, are negligibly small, the last two terms on the right hand side in eq. (9) are neglected. Thus:

$$f_A = f_g + \alpha_f(T - T_g) \quad (10)$$

where f_g is the fractional FV at glass transition, α_f is coefficient of volumetric thermal expansion of FV, and T_g is the glass transition temperature (T_g = 64°C).[30]

As f_A and V_f are functions of temperature, diffusion of byproducts in polymers, is effectively a thermally activated process.[31] The temperature-dependent specific volume for amorphous PLLA is calculated from PVT data,[32] although they are available for atmospheric and higher pressures, but not for vacuum. As the specific volume (V_s) versus temperature curves come progressively closer as pressure decreases, we assume that the data available for atmospheric pressure are a good approximation for the V_s values at vacuum. The occupied volume (V_o) is calculated as 1.3 times the van der Waals volume (V_w) of PLLA. We assume that the V_w is a negligibly weak function of temperature and compute it by the group contribution approach (we find V_w = 35.65 cm^3/mol = 0.4945 cm^3/gm).[33] f_g and α_f are calculated from Table IV and eq. (10), and the estimated values are 0.217 and 0.0004 K^{-1}, respectively.

Equation (11) is the modified form of eq. (8), and it yields the diffusivities of byproducts, which depend on the SSP time-dependent amorphous volume fraction (Φ_A (t)) and the isothermal SSP temperature (T):

TABLE IV
Estimation of Amorphous Fractional Free Volume (f_A) of PLLA

T (K)	V_s	V_o	$V_s - V_o$	$f_A = \frac{V_s - V_o}{V}$	$T - T_g$
313.2	0.8095	0.64285	0.16665	0.2059	–
333.0	0.8138	0.64285	0.17095	0.2101	–
353.0	0.8223	0.64285	0.17945	0.2182	16.0
373.3	0.83	0.64285	0.18715	0.2255	36.3
393.5	0.8389	0.64285	0.19605	0.2337	56.5
413.6	0.849	0.64285	0.20615	0.2428	76.6
433.6	0.853	0.64285	0.21015	0.2464	96.6

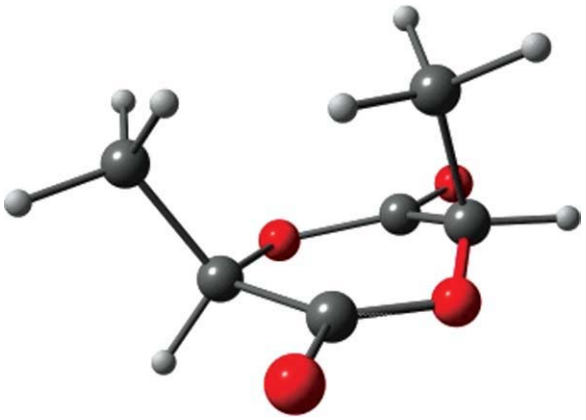

Figure 1 Minimized structure of L-lactide molecule, simulated by Materials Studio®. [Color figure can be viewed in the online issue, which is available at wileyonlinelibrary.com.]

$$D_j = RTA_j \exp\left[-\frac{B_j}{\left[0.217 + 4 \times 10^{-4}(T - T_g)\right]\Phi_A(t)}\right] \tag{11}$$

Estimation of A_j and B_j

In eqs. (11) and (8), the values of the constants, A_j and B_j, depend on the size and shape of the diffusing molecules.[29] B_j values for water and other molecules are obtained from the literature,[34] but for the lactide molecule, B_j is calculated by using the approach of Bixler et al.,[35] where eq. (12) is used to obtain the reduced molecular diameter required by the lactide molecule to diffuse in the amorphous PLLA system.

$$d' = d - \frac{\varphi^{1/2}}{2} \tag{12}$$

φ is FV per unit length of the repeat unit ($= V_{fu}/l_u$) measured along the chain axis, and d is molecular diameter; thus, $\varphi^{1/2}$ is the unoccupied intermolecular distance between two repeat units (i.e., an estimate of the mean value of the distribution of free distances in the amorphous region, about which, the chain can move without restriction). The molecular diameter (d = 3.836 Å) of the simulated lactide molecule (Fig. 1) is twice the radius of gyration (R_g), which is obtained as:

$$R_g = \sqrt{\frac{\sum_{i=1}^{n} M_i r_i^2}{\sum_{i=1}^{n} M_i}} \tag{13}$$

where M_i is a atomic weight of the ith atom and r_i is the distance of the atom from the center of mass. The length of the minimized structure of the simulated PLLA repeat unit (l_u) is 4.306 Å. The structure of a lactide molecule and that of a PLLA lactyl repeat unit (local energy minima have been reported by Tonelli[36]) are obtained via Accelrys' Materials Studio® software.[37] Molecular dynamics simulations using such software provide qualitative predictions of diffusivities.[38,39] We consider V_{fu}, the specific FV between two neighboring PLLA repeat units (= 0.026 cm^3/gm) in the semicrystalline morphology, as the difference between the total amorphous specific volume (V_A = 0.8 cm^3/g) and the crystalline specific volume (V_c = 0.775 cm^3/g) of PLLA.

$$V_{\text{fu}} = \frac{V_f(\text{cm}^3/\text{g}) \times 72(\text{g/mole repeat units})}{N_A(\text{repeat units/mole repeat units})} = 3.108\ \text{Å}^3/\text{repeat unit}.$$

Hence, $\varphi = V_{fu}/l_u$ = 0.722 Å^2 and $\varphi^{1/2}/2$ = 0.425 Å. Thus, the reduced diameter of a lactide molecule, calculated from eq. (12), is $d^l_{(LA)2}$ = 3.411 Å. Values of molecular diameters of various gas molecules are obtained from literature.[9,10]

Kulkarni and Mashelkar[29] have determined that $-\ln(B_j)$ is proportional to the square of the reduced molecular diameter. Therefore, we estimate the B_j value for lactide ($B_{(LA)_2}$ = 0.179), from the fit of $(d^l)^2$ with $-\ln(B_j)$ (Fig. 2).

No relation between A_j and size has been reported in the literature, although it is stated that A_j is related to the size of the molecule.[29] As A_j increases with decreasing molecular diameter, from known values, we obtain an empirical correlation, $\ln(A_j) = 70.89\ (d^i)^{-3} - 16.38$. Thus, $\ln(A_j)$ is an increasing function of $(d^i)^{-3}$ (corresponding to the reciprocal of the reduced or occupied molecular volume) of the gaseous molecules. A_j values for various gaseous molecules are listed in Table V. Thus, the diffusivity of j, D_{j,X_c}, at the instantaneous crystalline volume fraction, X_c (t) = 1 − Φ_A (t), can be related to $D_{j,A}$,

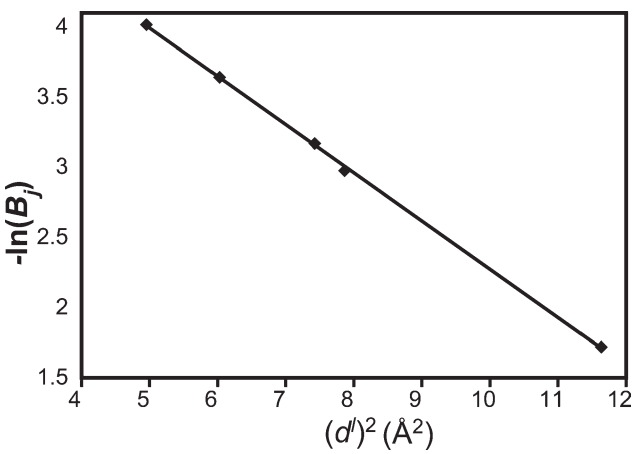

Figure 2 Relationship between B_j and effective diameter of small gaseous molecules.

TABLE V
A_j Values for Gaseous Molecules for Diffusivity Calculation

Molecule	(d^l) (Å)	A_j	ln (A_j)	$(d^l)^{-3}$ (Å^{-3})
Helium	2.225	5.80 E −05	−9.755	0.091
Water	2.455	6.20 E −06	−11.991	0.068
Nitrogen	2.725	4.00 E −06	−12.429	0.049
CO_2	2.805	1.50 E −06	−13.410	0.045
Lactide	3.411	4.37 E −07	−14.644	0.025

the corresponding diffusivity in 100% amorphous PLLA, X_c (t) and f_A, the amorphous FV fraction.

$$D_{j,X_c} = D_{j,A} \exp\left(-\frac{B_j}{f_A}\frac{X_c(t)}{1-X_c(t)}\right) \quad (14)$$

PLLA CRYSTALLIZATION KINETICS DURING SSP

To determine Φ_A during the SSP of PLLA, the kinetics of isothermal crystallization are considered using the Avrami equation:

$$\Phi_A(t) = 1 - X_c(t) = \exp[-(kt)^n] \quad (15)$$

where Φ_A is the volume fraction of amorphous phase at a given SSP time, n is the Avrami exponent, and k is the coefficient, which depends on temperature. We estimate the Avrami coefficients using representative experimental DSC crystallinity data,[26] obtained during SSP. The values for $k = 5 \times 10^{-6}$ s^{-1} and $n = 2.75$, respectively, at 150°C are obtained by fitting eq. (20) to our experimental data.

Values of n in the range 0.4–5.4 are reported in the literature,[40–47] which correspond to effects of purity,[41] stereospecificity,[41–43] mode of crystallization (isothermal[44] or nonisothermal[40]), characterization methods for estimating these values,[45,46] or the presence of a nucleating agent.[47] The effect of MW on the crystallization rate has been considered explicitly by Mano et al.,[40] who have found Avrami parameters, $k = 2.6 \times 10^{-3}$ and $n = 2.8$, for $\overline{M_n} \sim 86{,}000$ Da, and $k = 3.0 \times 10^{-3}$ and $n = 2.2$, for $\overline{M_n} \sim 269{,}000$ Da.

In contrast, our estimates of the Avrami parameters are for the case of crystallization during SSP. A fundamental difference between this crystallization and those described above is the high final (infinite time) crystallinity, achieved during step-growth SSP of PLLA. This high an X_c has also been observed during the step-growth SSP of PLLA, reported by Moon et al.[21] as well as during the slower, long-time ring opening polymerization reported by Nijenhuis et al.[48] Therefore, there appears to be a synchronization between the polymerization and crystallization kinetics, which enhances chain folding at the expense of entanglement. This behavior requires further study for a deeper insight.

Figure 3 depicts the fit of eq. (15) to experimental X_c. Before SSP, the prepolymer is of initial $X_{c0} \sim 68\%$ and $\overline{M_{n0}} \sim 10{,}200$ Da. As it undergoes SSP at 150°C under vacuum, the X_c increases to >90%, and $\overline{M_n}$ increases to ~ 150,000 Da.

After having described the physical effects of byproduct diffusion and crystallinity, we now describe the chemistry aspects, beginning with the determination of initial concentrations of the —OH and —COOH end-groups.

INITIAL CONCENTRATIONS OF PLLA REACTIVE END GROUPS

Determination of initial concentrations of hydroxyl and carboxylic acid end groups is essential for the functional group approach, as these concentrations enable determination of the SSP process kinetics. We have made fluoroderivaties of both, hydroxyl and carboxylic acid end-groups, followed by ^{19}F-NMR, for PLLA of different MW. This technique has been successfully demonstrated in the literature, for PET[49] and for end groups determination for monodisperse polystyrene.[50]

Determination of acid groups in PLLA

The fluoroderivatization of the terminal acid groups is carried out by DCC mediated esterification with HFIP, as per eq. (16).

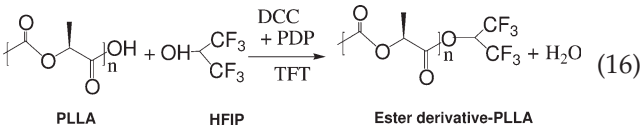

(16)

From the ^{19}F-NMR analysis spectra, the integration corresponding to the $\delta \approx -73$ ppm [d, 6F] peak for the fluoroester, relative to the TFT peak at $\delta \approx -62.9$ ppm [s, 3F], yields the relative quantification of the

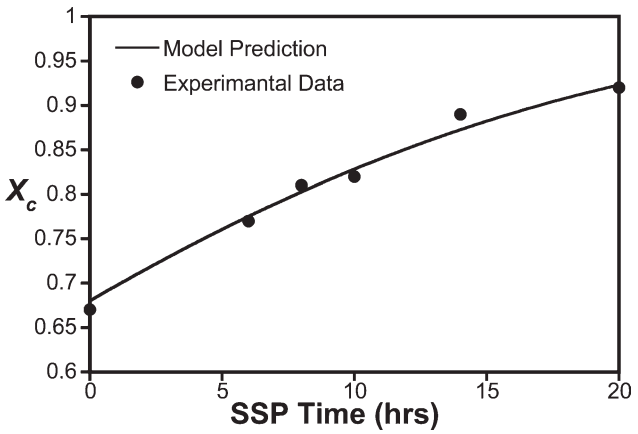

Figure 3 Comparison of variation in X_c during SSP of PLLA, at 150°C.

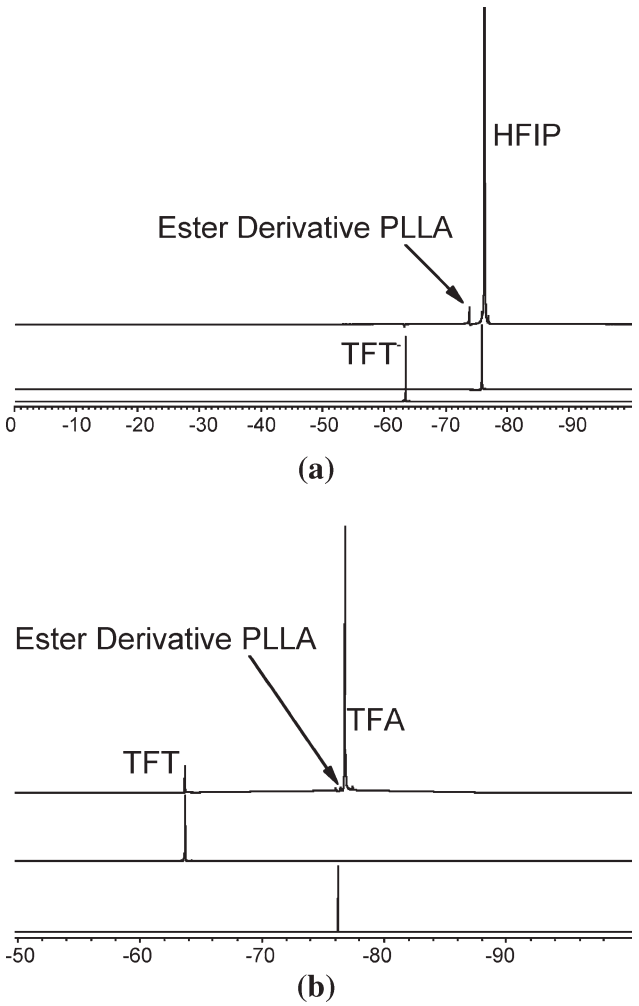

Figure 4 ^{19}F-NMR of PLLA fluoroester: (a) to determine the terminal carboxyllic acid groups; and (b) to determine the terminal hydroxyl groups.

terminal acid groups [Fig. 4(a)]. In this method, the ratio of the intensities is proportional to the ratio of molar concentrations of the fluorinated —COOH group and the known reference (TFT).

Determination of hydroxyl end-groups in PLLA

The hydroxyl end-groups are fluoroderivatized by esterification with TFA, as shown in eq. (17).

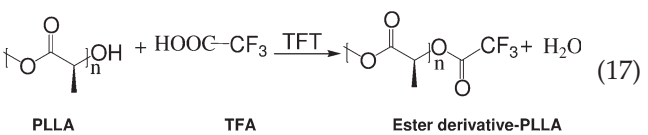

(17)

^{19}F-NMR analysis is carried out, where the integration corresponding to the $\delta \approx -75.9$ ppm [s, 3F] peak for the fluoroester, relative to the peak of TFT at $\delta \approx -62.9$ ppm [s, 3F], yields the relative quantification of the terminal hydroxyl groups [Fig. 4(b)].

Correlation of ^{19}F-NMR analyses with prepolymer MW data

We have also calculated the initial end group concentrations (assuming that $C^0_{OH} = C^0_{COOH}$) and number of ester groups based on the initial MW, M_{n0}, obtained by GPC analysis.

$$C^0_{OH} = \frac{\rho}{\overline{M_{n0}}}, \quad \overline{M_{n0}} = \frac{C^0_{COO}}{C^0_{OH}} M_0 \tag{18}$$

where M_0 is weight of one monomer repeat unit (72 Da). For the prepolymer of $\overline{M_{n0}} \sim 10{,}200$ Da, this yields $C^0_{OH} = C^0_{COOH} = 0.124$ mol/L.

In comparison, the estimated initial hydroxyl end groups concentrations, C^0_{OH}, and carboxylic end groups, C^0_{COOH}, of prepolymer from ^{19}F-NMR techniques are found as 0.4694 mol/L and 0.4572 mol/L, respectively. Thus, correction factors 0.264 for C_{OH} and 0.271 for C_{COOH} need to be incorporated into concentrations estimated from the relative ^{19}F-NMR peak intensities of the fluoroesters. As verified in the "calculation of $\overline{M_n}$" Section [eq. (28)], we find that these correction factors are consistent with other calculations, which validates their application.

FORMULATION FOR REACTION RATE CONSTANTS

We determine next, the kinetics parameters.

Rate constant for polycondensation reaction (k_1)

From Table III, reaction no. 2, the rate expression for formation (consumption) of —OH, is modified to yield an ODE, which can be solved by assuming that the initial concentrations of water are zero, at the surface of the pellet. This assumption has been made to mimic the experimental condition, where the pellet is exposed to high vacuum at 105°C for 2 h before performing SSP. The solution steps are as follows (reference time, $\tau = 20$ h, as SSP experiments are performed for 20 h):

$$\frac{dC_{OH}}{dt} = k_1 \frac{2\tau C^2_{OH}}{\Phi_A X^2_n} \tag{19}$$

$$C_{OH} = C^0_{OH} \times (1 - x) \tag{20}$$

$$C_{COO} = C^o_{COO} + C^o_{OH} x \tag{21}$$

Expressing the differential equation in terms of conversion, x,

$$\frac{dx}{dt} = k_1 \frac{2\tau \left(C^0_{OH}\right)^2}{\Phi_A X^2_n} (1 - x)^2 \tag{22}$$

Converting it to integral form,

TABLE VI
Evaluation of Polycondensation Rate Constant (k_1)
[Rewriting eq. (23) in the Form, $y = k_1x$]

Time (h)	M_n	x	Integral value y (LHS)	Integral value x (RHS)
0	10,200	0.000	0	0
3	28,900	0.646	0.21×10^5	23.46
5	76,800	0.867	4.17×10^5	46.95
10	95,800	0.893	11.52×10^5	175.22
15	109,600	0.907	19.32×10^5	698.96

$$\frac{1}{\left(C^0_{OH}\right)^2}\int_0^x \frac{X_n^2 dx}{(1-x)^2} = 2\tau k_1 \int_0^t \frac{dt}{\Phi_A} \tag{23}$$

where the degree of polymerization, X_n, has been equated to $C_{COO}/C_{OH} \cdot x$ represents the conversion of hydroxyl end groups during SSP, and C^0_{OH} and C^0_{COOH} are the initial concentrations (i.e., the concentrations in the prepolymer) of hydroxyl end groups and bonded ester groups, respectively.

We integrate both sides over the initial SSP time period ($\leq$10 h), in which range, the effects of degradation and diffusion hindrances are less, and chemical reaction effectively controls the SSP process. $\overline{M_n}$ is determined by GPC analysis of representative SSP experiments at 150°C under vacuum (Table VI). The integral [LHS of eq. (23)] is determined numerically, using the "quadl" routine in MATLAB®.

The slope of the plot between two integral values (y and x, by rewriting eq. (23) in the form, $y = k_1x$) at various time steps, yields the rate constant, $k_1 =$ 152.4 L/mol s.

Rate constant for backward reaction (k_2)

Above T_g, only amorphous polymer segments (but not entire chains) possess translational degrees of freedom (reaction 1, Table II). Therefore, in comparison with melt polymerization, the chain mobility during SSP is very low, due to the solid state of the polymer matrix. The effect of chain mobility has been determined by Kang,[28] using reptation theory and an Arrhenius-type relation for PET. Therefore, the rate constants for the reactions between the reactive polymer chains can also be expressed as functions of the chain mobility and the activation energy of the reaction [eq. (24)].

$$k_1 = A_1 \frac{X_{n0}^2}{X_n^2} exp\left[-\frac{Ep}{RT}\right] exp\left[-\frac{E_1}{RT}\right] \tag{24}$$

where A_1 is the prefactor, X_{n0} is the degree of polymerization of the reference state (initial degree of polymerization, i.e., that of PLLA prepolymer), X_n is the instantaneous degree of polymerization during SSP, E_1 is the intrinsic activation energy of the reaction, and E_p is activation energy for translational motion of the reactive end groups.

The rate constant for the backward reaction can be written as:

$$k_2 = \frac{A_1}{K_c} exp\left[-\frac{E_1}{RT}\right] \tag{25}$$

where the equilibrium constant (K_c) for the polycondensation reaction can be determined as[51]:

$$X_n = K_c^{0.5} + 1 \sim K_c^{0.5} \tag{26}$$

The expression for k_2 is obtained by dividing the expression for k_1 by the translational and chain mobility terms.

$$k_2 = \frac{k_1 exp\left(\frac{E_p}{RT}\right)}{K_C X_{n0}^2} \tag{27}$$

The values used for E_p for calculation of k_2 are those reported for the folding of PLLA polymer chains (which basically corresponds to molecular segment motion) at various temperatures.[52] A linear variation is observed with respect to temperature, as shown in Figure 5. From eqs. (24)–(27), the rate constant at 150°C, $k_2 = k_1/17{,}400$.

Rate constant for depolymerization (k_3) (lactide formation)

This rate constant is determined by using our experimental degradation data for PLLA.[26] The system is considered to be completely amorphous, and the initial MW of the sample is $\sim$ 9400 Da (which is close to the prepolymer MW, 10,200). The degradation is assumed to be pseudo-first order in hydroxyl

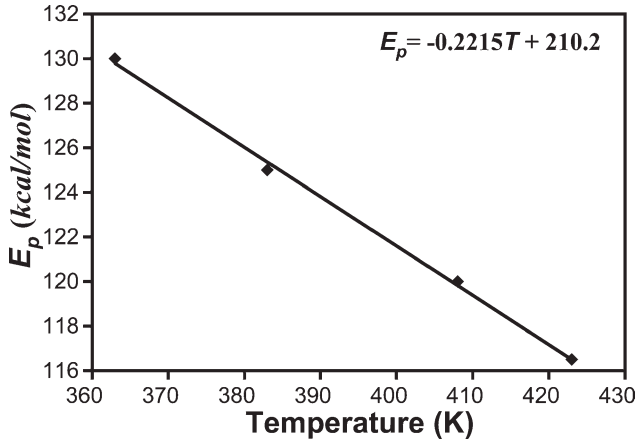

Figure 5 E_p versus temperature plot, for semicrystalline PLLA.

groups. Hence, the rate of appearance of lactide is constant. A linear fit in the plot of lactide weight versus time (up to 4 h, during which the lactide amount is quantifiable) yields the value of the slope, which, when divided by the hydroxyl group concentration, equals the rate constant ($k_3 = 6.91\ h^{-1}$) for degradation.

Thus, the parameters, k_1, k_2, and k_3, are optimized to only the initial SSP data ($\leq$10 h).

CALCULATION OF $\overline{M_n}$

The hydroxyl and carboxyl group concentrations have been obtained as function of time and across the radius of the particle, by solving the equations in Table III. The degree of polymerization (X_n) of the polymer chains can be obtained from eq. (28).

$$X_n = \frac{C_{(LA)-OH} + C_{HOOC-(LA)-OH} + C_{(LA)-COOH}}{\frac{[C_{(LA)-OH} + C_{(LA)-COOH}]}{2}} \quad (28)$$

$$\overline{M_n} = M_0 X_n \quad (29)$$

The implementation of eq. (28) yields similar results, irrespective of whether or not the correction factors are implemented for determining end-group concentration via ^{19}F-NMR. However, eq. (18) should yield the same value of X_{n0}, as that obtained when applying eq. (28) at the beginning of SSP. This is achieved by using the correction factors. The X_{n0} is essentially the initial condition input to equations in Table III, which in combination with eq. (28), provides the estimates of the MW during SSP. Thus, incorporating the correction factors in the determination end-group concentrations makes the framework self-consistent.

The expression for $\overline{M_n}$, the average MW for spherical PLLA particles, is derived by recognizing that the volume of a PLLA molecule is directly proportional to its local (or individual) $M_n(r)$ (described in the Appendix), which is a function of its radial distance from the particle center [eq. (30)] and found consistent with $\overline{M_n}$ derived by Ye and Choi.[12,13]

$$\overline{M_n} = \frac{R^3/3}{\int_0^R \frac{r^2}{M_n(r)} dr} \quad (30)$$

In contrast, Kim and Jabarin[27] have been calculated the instantaneous $\overline{M_n}$, averaged over the entire pellet, by integration over all positions [eq. (31)].

$$\overline{M_n} = \frac{\int_0^R r^2 M_n(r) dr}{R^3/3} \quad (31)$$

We now examine the results of our computation.

TABLE VII
Comparative Diffusivity Values in PLLA Estimated by FFV Approach

Diffusing molecule	Temperature (°C)	D_{j,X_c} via FFV (cm^2/s)
Lactide	150	7.3×10^{-8}
Lactide	135	7.2×10^{-8}
Lactide	125	7.0×10^{-8}
Lactide	100	6.8×10^{-8}
Water	150	1.48×10^{-6}
Water	135	1.47×10^{-6}
Water	125	1.46×10^{-6}
Water	100	1.43×10^{-6}
Helium	100	1.66×10^{-5}
Nitrogen	100	1.80×10^{-6}
Oxygen	100	9.70×10^{-6}
Argon	100	9.81×10^{-6}

RESULTS AND DISCUSSIONS

Diffusivity computations

Table VII lists the values of diffusion coefficients, D_{j,X_c}, as estimated by the FV method [eq. (14)], for lactide, water, helium, nitrogen, and oxygen molecules in the PLLA matrix, at various temperatures. These values are at fixed $X_{c0} = 0.68$, of the PLLA prepolymer. However, D_{j,X_c} values decrease with temperature. This is expected, because at lower temperatures, the FV between the PLLA chains, decreases significantly, increasing the hindrance to the diffusent molecules. We have explicitly used in our modeling framework, the FV estimates, directly and quantitatively.

The values of the estimated diffusion coefficients of the investigated gases in PLLA polymer decrease with the gas in the order: He > Ar > O_2 > N_2 > H_2O > lactide. This is also the order of increasing "kinetic" molecular diameters of these gases. Thus, the rates of diffusion of penetrant molecules depend on the sizes of these molecules. This is consistent with A_j and B_j being strong functions of the molecular diameters of the diffusent molecules (Table V and Fig. 2).

We now examine the effects of the polymer properties and SSP reaction conditions, on the diffusivities of the byproducts such as water and lactide. In our modeling framework, we have accounted for the diffusivity variation as SSP proceeds, by accounting for the dependence of the FV on the SSP time.

Effect of PLLA prepolymer MW

First, the effect of prepolymer MW has been examined by varying the initial T_g of the PLLA prepolymer, in eq. (11) at the SSP temperature of 150°C, for initial $X_c = 68\%$. From Figure 6, both, D_W and $D_{(LA)_2}$ decrease very slightly with an increase in initial T_g. This small variation in the diffusivities with initial

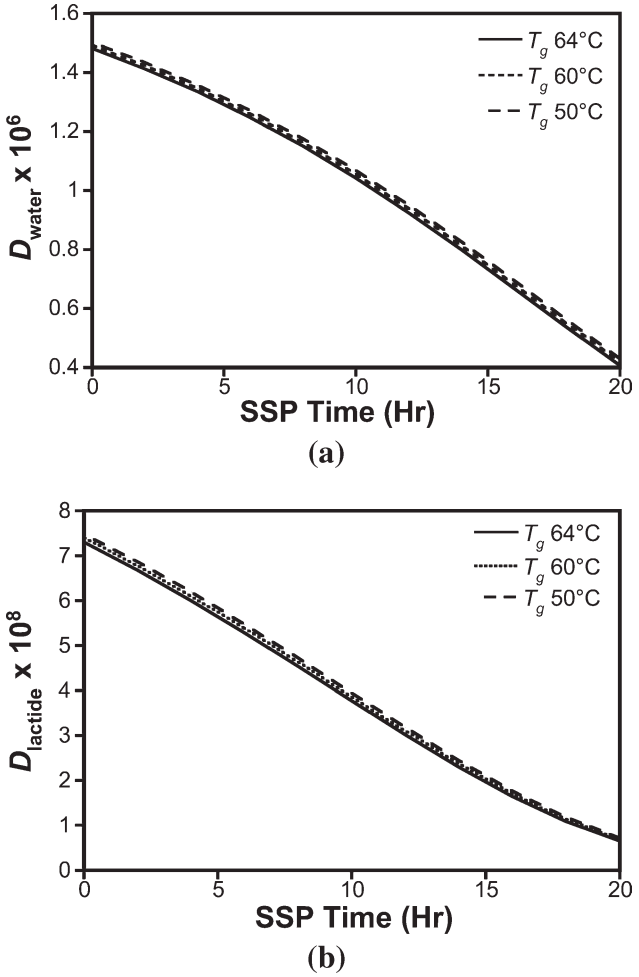

Figure 6 Prediction of byproducts diffusivity (a) water and (b) lactide, during the SSP of PLLA at 150°C, for different T_g of PLLA prepolymer.

T_g may be due to the corresponding variation in the free-volume-dependent segmental mobility of PLLA. In case of low MW PLLA (low T_g), the high concentration of chain ends, leads to greater free-volume, and thus, greater segmental mobility. As PLLA MW increases (higher T_g), the concentration of chain ends decreases during SSP, and in turn, the PLLA FV decreases. As a result, byproduct diffusivity decreases as SSP progresses, as presented in Figure 6. At higher MW, when the concentration of chain ends is low, diffusivity is relatively independent of MW; in the figure, the gaps between the D values for different T_g, decrease, as SSP time increases. Also, as SSP progresses, X_c increases, which decreases diffusivity. The impermeable crystallites increase the tortuosity of the path taken by the diffusents through PLLA. Also, due to increase in X_c, the segmental motion of PLLA chains in amorphous regions is restricted, and hence, the penetrant molecules are hindered from jumping into a neighboring microcavity; thus, both effects tend to reduce the gas diffusivity.

Effect of SSP temperature

The diffusion of byproducts (water and lactide) in PLLA is a thermally activated process,[30] and the diffusion coefficient is, therefore, expressed as:

$$D = D_0 exp\left(-\frac{E_d}{RT}\right) \tag{32}$$

E_d is the activation energy of diffusion of byproducts, and D_0 is a constant.[30] According to eq. (32), gas diffusion coefficients typically increase with increase in temperature. Computed values of both, D_W and $D_{(LA)_2}$, increase with SSP temperature as expected and decrease with SSP time (Fig. 7).

Effect of initial crystallinity of PLLA prepolymer

Figure 8 shows that the D value during SSP, strongly depends on the initial X_c of the PLLA

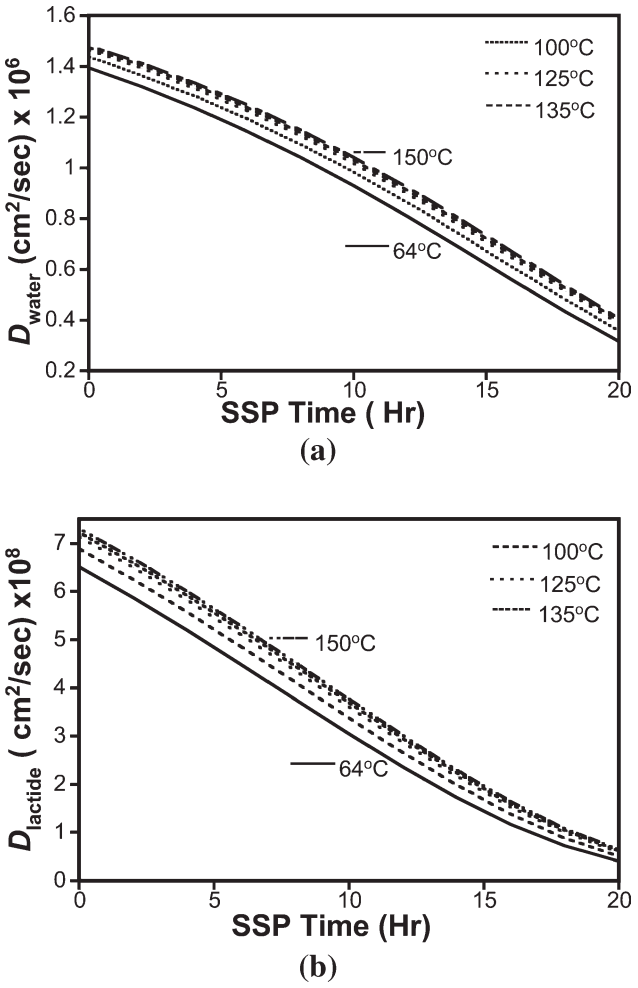

Figure 7 Prediction of byproducts diffusivity (a) water and (b) lactide, during the hypothetical SSP of PLLA at different SSP temperatures. Initial X_c (X_{c0}) of PLLA prepolymer = 68%. Avrami parameters are assumed to be the same as those at 150°C. Rate constants estimated by eqs. (24)–(27).

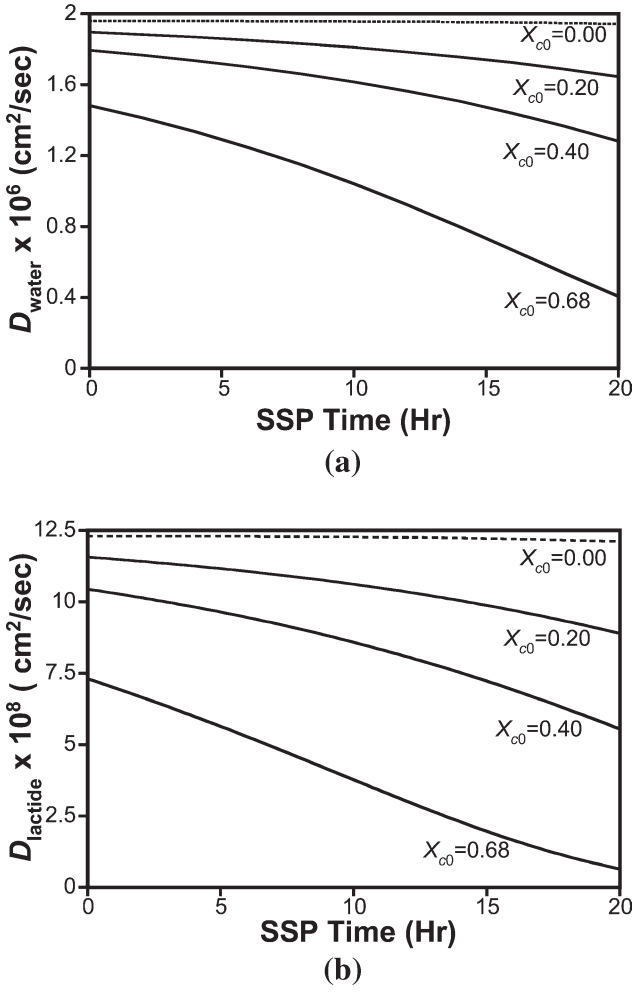

Figure 8 Prediction of byproducts diffusivity (a) water and (b) lactide, during the SSP of PLLA at 150°C, for different X_{c0} of PLLA prepolymer.

prepolymer. For the amorphous ($X_c = 0$) PLLA prepolymer, the diffusivity does not change during SSP; however, in case of semicrystalline prepolymer, during SSP, D reduces significantly with increase in X_{c0}, the initial X_c. $D_{(LA)_2}$ decreases more rapidly than D_W, possibly because the smaller water molecules, feel less hindered, during diffusion.

Effect of crystallinity during SSP

On the basis of the fitted parameters (Fig. 3), k and n of the Avrami equation, we estimate the X_c of the PLLA, during and after SSP. Figure 9 presents the computed X_c variation with SSP time at 150°C. Here, we find that the amorphous PLLA prepolymer does not undergo significant crystallization, and only up to 5% increase in X_c is predicted, after 20 h SSP. On the other hand, in case of high initial X_c, further crystallization occurs more rapidly, and X_c increases correspondingly. Hence, initial X_c in prepolymer, induces further crystallization during SSP. Therefore,

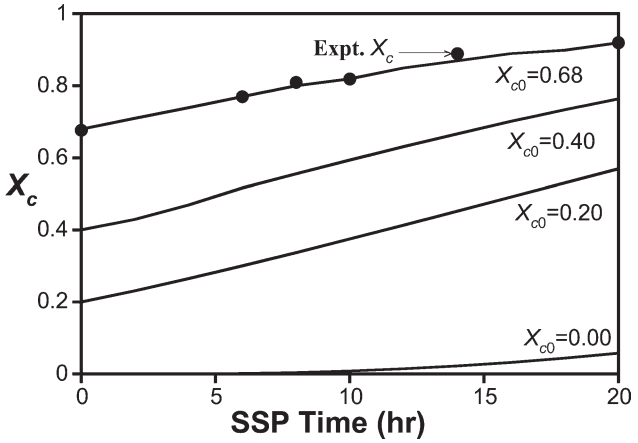

Figure 9 Prediction of X_c during the SSP of PLLA at different initial X_{c0} of PLLA prepolymer.

reaction progress is influenced by the crystallization history and the time of prepolymer crystallization.

X_{c0} significantly influences the SSP rate, because it controls critical reaction parameters such as effective end-group concentrations and byproduct diffusion. Thus, there are competing effects of X_c on the SSP rate. On the one hand, higher X_c enhances the SSP rate, by increasing the effective concentration of reactive end groups, which generally cannot exist in the crystalline phase. On the other hand, as SSP proceeds, the mobility of the polymer chains decreases because of increase in MW and X_c, and this hinders the escape of byproducts; i.e., diffusivity decreases with increase in X_c.

Thus, in byproduct diffusion limited reactions, SSP rate decreases with increasing X_c, whereas in reaction controlled kinetics, the rate increases with increase in X_c. We find here that the SSP rate depends on both factors. In the initial few hours, the SSP rate increases, possibly due to generation of sufficient crystallinity, which causes an increase in the

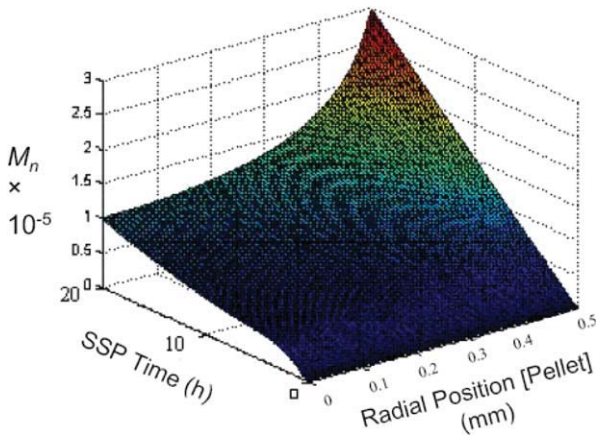

Figure 10 Surface plot of local M_n as function of SSP and radial position within the pellet. [Color figure can be viewed in the online issue, which is available at wileyonlinelibrary.com.]

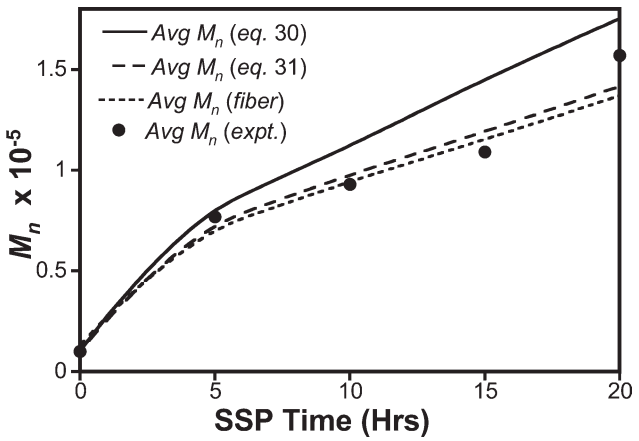

Figure 11 Result of fitting the simulated $\overline{M_n}$ (Avg. M_n) during the SSP in comparison with the experimental data. Lines are the $\overline{M_n}$ calculated for both spherical [eqs. (30) and (31)] and cylindrical (fiber) geometry. Filled circles represent the corresponding $\overline{M_n}$ values obtained from experiment.

effective concentrations. Subsequently, the rate of depolymerization dominates over the polymerization reaction. At this stage, byproduct (water) molecules are hindered from diffusing out of the reaction system. Subsequently, these participate in the depolymerization process. Thus, at this stage, the diffusion process dominates over chemical reaction.

MW estimates during SSP

Figure 10 presents simulation results predicting the MW during the entire 20 h SSP duration at 150°C, as function of time and position in a PLLA spherical pellet. A higher SSP rate is obtained at the surface of the pellet, than at its center, because the surface location provides for easy diffusion of the byproducts from the pellet.

The $M_n(r)$ values are averaged for all the positions in the pellet, which is assumed to be spherical. The predicted $\overline{M_n}$ values calculated by using eqs. (30) and (31) have been validated by the experimental SSP data at 150°C,[26] and a representative result is presented in Figure 11. Equation (30) predictions are slightly higher than the experimental $\overline{M_n}$; however, the trends for all the cases, are similar, and lie in the permissible error range, with respect to experimental data. However, although the difference is very slight, the cylindrical geometry consistently yields a lower MW, because there is one lesser dimension available for the MW-reducing diffusents such as water, to exit the system.

SUMMARY AND CONCLUSIONS

We have objectively and comprehensively modeled the SSP process for PLLA, by using a functional group approach. We have used a combination of various techniques for estimation of model parameters:

- Suitably fitting the kinetics model equations to bulk average experimental MW during the first few hours of the SSP (when the SSP process is primarily controlled by chemical reaction) and to the initial end-group concentration data have yielded the rate constants of the contributing reactions. These rate constants have been applied throughout the SSP process.
- Diffusion parameters have been estimated via FV approach. This framework provides estimates of diffusivities of reaction byproducts and of other gases.
- Determination of the Avrami constants has enabled estimation of the dynamic crystallinity during SSP. This has enabled determination of the effective amorphous end-group concentrations and of the dependence of the diffusivities on SSP time, as they depend on the time-dependent crystallinity.
- We have successfully quantified reactive end groups (hydroxyl and carboxylic) by converting them into fluorinated ester groups and using ^{19}F-NMR spectroscopy. We have determined and used self-consistent empirical correction factors, by correlating with $\overline{M_{n0}}$ the prepolymer MW, obtained via GPC.

Based on these techniques,

- Our framework provides guidelines to estimate the final product crystallinity on the basis of PLLA prepolymer crystallinity, X_{c0}.
- MW can be predicted as function of SSP time, for both, spherical and cylindrical geometries. The MW for the spherical particle is always higher than that for a cylindrical geometry, as there are more dimensions, through which the byproducts can diffuse out. As expected, the MW increases, from the center to the surface, for both geometries.

Our methodology uses initial bulk average $\overline{M_n}$ values, to estimate reaction rate constants. However, our model estimates of SSP MW are fundamentally objective, based on first principles, account for all the relevant concurrently occurring phenomena, and correspond well with the experimental results. This framework can be extended to consider variations such as step-changes in temperature, inclusions of plasticizers or nanofillers as well as influence of inert carrier gases. Our contribution provides a fundamental understanding of the various physical and chemical facets of SSP and is a first report, quantifying the same for the case of PLLA.

NOMENCLATURE

A_j	Prefactor (cm^3/kmol/h)
B_j	Jump factor
C_j	Concentrations based on the entire volume of the pellet (mol/cm^3)
C_j^i	Effective concentrations in the amorphous region (mol/cm^3)
D_j	Diffusion coefficient of molecule type j (cm^2/s)
D_{j,X_c}	Diffusivity at instantaneous crystalline volume fraction (cm^2/s)
$D_{j,A}$	Diffusivity at 100% amorphous PLLA (cm^2/s)
d	Molecular diameter (Å)
E_1	Intrinsic activation energy of the reaction (kJ/kmol)
E_p	Activation energy for translational motion of the reactive end groups (kJ/kmol)
E_d	Activation energy of diffusion of byproducts (kJ/kmol)
f_A	Fractional free volumes of the amorphous phase (cm^3)
$f_{(LA)_2}$	Fractional free volumes of lactide (cm^3)
f_W	Fractional free volumes of water (cm^3)
f_g	Fractional free volume at glass transition (cm^3)
G_j (t)	Generation rate for species, j = nondiffusing component (mol/cm^3/h)
G_j^i (t)	Generation rate, j = nondiffusing component in amorphous phase (mol/cm^3/h)
k_1	Rate constant for polycondensation reaction (L/mol/s^{-1})
k_2	Rate constant for backward reaction (L/mol/s^{-1})
k_3	Rate constant for depolymerization (h^{-1})
k	Avrami coefficient (s^{-1})
K_c	Equilibrium constant for the polycondensation reaction
l_u	Length of the minimized structure of the simulated PLLA repeat unit (Å)
M_i	Atomic weight of the ith atom (g/mol)
M_n (r)	Local number average molecular weight at a radial position (Da, g/mol)
$\overline{M_n}$	Number average MW for spherical PLLA particles (g/mol)
$\overline{M_{n0}}$	Molecular weight of prepolymer (Da, g/mol)
M_0	Weight of one lactic acid monomer repeat unit (g/repeat unit)
$\overline{M_w}$	Weight average molecular weight (Da, g/mol)
m	Geometry of the particle
N_A	Repeat units/moles repeat units
n	Avrami exponent
r	Radial distance (mm)
r_s	Particle radius (mm)
R	Ideal gas constant
R_g	Radius of gyration (Å)
r_i	Distance of the atom from the center of mass (Å)
t	SSP reaction time (h)
T	Temperature (K)
T_g	Glass transition temperature (K)
V_f	Effective fractional free volume (cm^3)
V_s	Specific volume (cm^3/mol)
V_o	Occupied volume (cm^3/mol)
V_w	van der Waals volume (cm^3/mol)
$V_{\underline{fu}}$	Specific free volume between two neighboring PLLA ($Å^3$/repeat unit)
V_A	Amorphous specific volume (cm^3/g)
V_c	Crystalline specific volume (cm^3/g)
X_c	Crystalline volume fraction (cm^3/cm^3)
X_{c0}	Prepolymer crystalline volume fraction (cm^3/cm^3)
X_n	Degree of polymerization

Greek symbols

Φ_A	Amorphous fraction (cm^3/cm^3)
$\Phi_{(LA)_2}$	Volume fractions of lactide (cm^3/cm^3)
Φ_W	Volume fractions of water (cm^3/cm^3)
α_f	Coefficient of volumetric thermal expansion of free volume (K^{-1})
φ	Free volume per unit length of the repeat unit ($Å^2$)
ρ	Density of PLA prepolymer (g/cm^3)
τ	Reference time for SSP (h)

APPENDIX: DERIVATION FOR $\overline{M_n}$ FOR SPHERICAL PLLA PARTICLES

The expression for $\overline{M_n}$, the average MW for spherical PLA particles, is derived by recognizing that the volume of a PLLA molecule is directly proportional to its local $M_n(r)$, which is a function of its radial distance from the particle center:

Assumption: volume of polymer molecule, $V \propto M_n(r)$

Hence, $V = c\, M_n(r)$ (where c is the proportionality constant)

Now, the number of molecules in unit volume of PLLA = $1/(c\, M_n(r))$.

Hence, the average molecular weight for spherical particle with radius (r) can be written as:

$$\overline{M_n} = \frac{\int_0^R 4\pi r^2 \frac{1}{cM_n(r)} \times M_n dr}{\int_0^R 4\pi r^2 \frac{1}{cM_n(r)} dr} = \frac{\frac{R^3}{3}}{\int_0^R \frac{r^2}{M_n(r)} dr}$$

References

1. Garlotta, D. J Polym Environ 2001, 9, 63.
2. Stridsberg, K. S.; Maria, R.; Albertsson, A.-C. Adv Polym Sci 2002, 157, 41.
3. Albertsson, A. C.; Varma, I. K. Biomacromolecules 2003, 4, 1466.
4. Vouyiouka, S. N.; Karakatsani, E. K.; Papaspyrides, C. D. Prog Polym Sci 2005, 30, 10.

5. Chen, S.-A.; Chen, F.-L. J Polym Sci Part A: Polym Chem 1987, 25, 533.
6. Duh, B. J Appl Polym Sci 2002, 83, 1288.
7. Mallon, F. K.; Ray, W. H. J Appl Polym Sci 1998, 69, 1233.
8. Lucas, B.; Seavey, K. C.; Liu, Y. A. Ind Eng Chem Res 2007, 46, 190.
9. Bikiaris, D. N.; Achilias, D. S.; Giliopoulos, D. J.; Karayannidis, G. P. Eur Polym J 2006, 42, 3190.
10. Achilias, D. S.; Bikiaris, D. N.; Karavelidis, V.; Karayannidis, G. P. Eur Polym J 2008, 44, 3096.
11. Gostoli, C.; Pilati, G.; Sarti, G. C.; Giacomo, B. D. J Appl Polym Sci 1984, 29, 2873.
12. Gross, S. M.; Roberts, G. W.; Kiserow, D. J.; DeSimone, J. M. Macromolecules 2001, 34, 3916.
13. Ye, Y.; Choi, K. Y. Ind Eng Chem Res 2008, 47, 3687.
14. Srinivasan, R.; Desai, P.; Abhiraman, A. S.; Knorr, R. S. J Appl Polym Sci 1994, 53, 1731.
15. Srinivasan, R.; Almonacil, C.; Narayan, S.; Desai, P.; Abhiraman, A. S. Macromolecules 1998, 31, 6813.
16. Almonacil, C.; Desai, P.; Abhiraman, A. S. Macromolecules 2001, 34, 4186.
17. Kaushik, A.; Gupta, S. K. J Appl Polym Sci 1992, 45, 507.
18. Kulkarni, M. R.; Gupta, S. K. J Appl Polym Sci 1994, 53, 85.
19. Yao, K. Z.; McAuley, K. B.; Berg, D.; Marchildon, E. K. Chem Eng Sci 2001, 56, 4801.
20. Harshe, Y. M.; Storti, G.; Morbidelli, M.; Gelosa, S.; Moscatelli, D. Macromol Symp 2007, 259, 116.
21. Moon, S.-I.; Lee, C.-W.; Taniguchi, I.; Miyamoto M.; Kimura Y. Polymer 2001, 42, 5059.
22. Xu, H.; Luo, M.; Yu, M.; Teng, C.; Xie, S. J Macromol Sci Phys 2006, 45, 681.
23. Shinno, K.; Miyamoto, M.; Kimura, Y; Hirai, Y.; Yoshitome, H. Macromolecules 1997, 30, 6438.
24. Chen, S.; Chen, F. J Polym Sci Part A: Polym Chem 1987, 25, 533.
25. Zimmerman, J.; Kohan, M. J Polym Sci Part A: Polym Chem 2001, 39, 2565.
26. Katiyar, V. Ph.D. Thesis, Indian Institute of Technology Bombay, Mumbai, India, 2008.
27. Kim, T. Y.; Jabarin, S. A. J Appl Polym Sci 2003, 89, 213.
28. Kang, C.-K. J Appl Polym Sci 1998, 68, 837.
29. Kulkarni, M. G.; Mashelkar, R. A. Chem Eng Sci 1983, 38, 925.
30. Pan, P.; Kai, W.; Zhu, B.; Dong, T.; Inoue, Y. Macromolecules 2007, 40, 6898.
31. Bharadwaj, R. K.; Boyd, R. H. Polymer 1999, 40, 4229.
32. Sato, Y.; Inohara, K.; Takishima, S.; Masuoka, H.; Imaizumi, M.; Yamamoto, H.; Takasugi, M. Polym Eng Sci 2000, 40, 2602.
33. Ghosal, K.; Freeman, B. D. Polym Adv Technol 1994, 5, 673.
34. Devotta, I.; Mashelkar, R. A. Chem Eng Sci 1993, 48, 1859.
35. Bixler, H. J.; Michaels, A. S. J Polym Sci 1961, L, 413.
36. Tonelli, A. E. Macromolecules 1992, 20, 3581.
37. Accelrys® Inc. Polymerizer Module of InsightII® Software and Amorphous Cell Module in Material Studio® Software; Accelrys® Inc.: San Diego, California, USA, 2004.
38. Charati, S. G.; Stern, S. A. Macromolecules 1998, 31, 5529.
39. Brant, D. A.; Tonelli, A. E.; Flory, P. J. Macromolecules 1969, 2, 2028.
40. Mano, J. F.; Wang, Y.; Viana, J. C.; Denchev, Z.; Oliveira, M. J Macromol Mater Eng 2004, 289, 910.
41. Schmidt, S. S.; Millmyer, M. A. J Polym Sci Part B: Polym Phys 2001, 39, 300.
42. Kolstad, J. J. J Appl Polym Sci 1996, 62, 1079.
43. Anderson, K. S.; Hillmyer M. A. Polymer 2006, 47 2030.
44. Iannace, S.; Nicolais, L. J Appl Polym Sci 1997, 64, 911.
45. Zhang, J.; Tsuji, H.; Noda, N.; Ozaki, Y. Macromolecules 2004, 37, 17.
46. Cho, J.; Baratian, S.; Kim, J.; Yeh, F.; Hsiao; B. S.; Runt, J. Polymer 2003, 44, 711.
47. Liao, R.; Yang, B.; Yu, W.; Zhou, C. J Appl Polym Sci 2007, 104, 310.
48. Nijenhuis, A. J.; Grijpma, D. W.; Pennings, A. J Polym Bull 1991, 26, 71.
49. Ma, Y.; Agarwal, U. S.; Sikkema, D. J.; Lemstra, P. J. Polymer 2003, 44, 4085.
50. Rajan, M.; Cotiuga, I.; Ma, Y.; Picchioni, F.; Agarwal, U. S. e-Polymer 2003, 46, 1.
51. Duda, A.; Penczek, S. In Polymers as Biomaterials; Shalaby, S. W., Hoffman, A. S., Ratner, B. D., Horbett, T. A., Eds.; Plenum Press: New York, 1984; Vol.371.
52. Iannace, S.; Maffezzoli, A.; Leo, G.; Nicolais, L. Polymer 2001, 42, 3799.